Low-energy photodetachment of O^-

Oleg Zatsarinny* and Klaus Bartschat†
Department of Physics and Astronomy, Drake University, Des Moines, Iowa 50311, USA
(Received 8 November 2005; published 22 February 2006)

The *B*-spline *R*-matrix method is used to investigate the low-energy photodetachment of $O^-(2p^5)$ for photon energies from threshold to 7 eV. We report a detailed study regarding the dependence of the predicted partial and total photodetachment cross sections on the scattering model and the accuracy of the target description. A multiconfiguration Hartree-Fock method with nonorthogonal term-dependent orbitals is employed to generate accurate representations of the target wave functions. Four close-coupling scattering models with a different number of target states in the expansion are used to explore the dependence of the calculated photodetachment cross sections on the polarization of the target. Our largest model for the *e*-O collision problem in the final state includes 60 states, namely 25 bound and autoionizing states of neutral oxygen derived from the $1s^22s^22p^4$, $2s^22p^3n\ell$, and $2s2p^5$ configurations, plus a set of pseudostates to partially account for the polarizability of the ground state $2p^4\ ^3P$ and the metastable $2p^4\ ^1D$ and ^1S states. We only find a small dependence of the calculated photodetachment cross section on the amount of target polarization accounted for, but a very strong dependence of the near-threshold results on the degree of short-range inner-core correlation incorporated in the target description.

DOI: 10.1103/PhysRevA.73.022714 PACS number(s): 32.80.Gc

I. INTRODUCTION

Photodetachment cross sections for O^- were measured a long time ago [1,2], but they still provide a challenge for theoretical interpretation. Atomic oxygen is an open-shell system where both short-range correlation and polarization effects are believed to be very important. An accurate representation of the oxygen target wave functions requires large configuration-interaction expansions and is further complicated by the strong term dependence of the valence orbitals. The correct treatment of the long-range dipole polarization requires an accurate representation of many coupled channels, including the target continuum spectrum. The latter is very important in the present case, because most ($\sim$75%) of the ground-state polarizability in atomic oxygen arises from coupling to the continuum [3].

Photodetachment cross sections for O^- are important for modeling various astrophysical objects. Atomic oxygen is one of the most abundant elements in the universe, and one of its important forms in space is the negative atomic oxygen ion. Absolute measurements of the O^- photodetachment cross sections by Smith [1] showed a sharp rise from threshold (1.47 eV) to a nearly constant value up to the highest energy of 3.10 eV accessible with the apparatus. A relative measurement with higher energy resolution, performed a few years later by Branscomb *et al.* [2], revealed additional steplike structure at the $O(^1D)$ threshold. Absolute values for the cross sections were generated through normalization to the data of Smith [1].

On the theoretical side, calculations performed by Garrett and Jackson [4], Henry [5], and Vo *et al.* [6] employed relatively simple three-channel collision approximations while accounting for correlation effects through semiempirical model polarization potentials. Although these calculations managed to reproduce the overall energy dependence of the measured cross sections, the differences obtained with the length and velocity forms of the electric dipole operator were as large as a factor of 2, thereby indicating that correlation effects were not included to a sufficient extent. Chase and Kelly [7] calculated the photodetachment cross sections in the extended energy region from threshold to 1.1 keV by means of many-body perturbation theory and predicted two strong resonances due to $2s \rightarrow 2p$ and $1s \rightarrow 2p$ excitations. They also found that the length form of the dipole matrix element yielded significantly smaller results than experiment. Finally, detailed *ab initio* calculations for O^- photodetachment were carried out by Miecznik and Greene [8] who used an eigenchannel *R*-matrix method. Their results exhibited a very different energy dependence compared to the earlier calculations and experiment [1,2]. Note, however, that Miecznik and Greene concentrated their efforts on the fine structure near the $O(2p^4\ ^3P_J)$ thresholds, where they obtained good agreement with relative measurements by Suzuki and Kasuya [9].

Recently, new *R*-matrix calculations of the near-threshold photodetachment cross sections for O^- were reported by Wu *et al.* [10], who used extensive multiconfiguration target wave functions and a 40-state close-coupling scattering model. Their results agree with the experimental data regarding the structure near the ^3P and ^1D thresholds, but once again the absolute values of the calculated cross sections were considerably larger than the experimental data.

The above calculations indicate a strong dependence of the low-energy photodetachment cross section on the correlation and polarization effects incorporated in the theoretical models, but they do not provide sufficient information regarding the convergence of the results obtained. The purpose of the present work therefore was to conduct a detailed in-

*Electronic address: oleg_zoi@yahoo.com
†Electronic address: klaus.bartschat@drake.edu

vestigation of the dependence of the predicted partial and total photodetachment cross section on the scattering model and the accuracy of the target description. The present calculations were carried out with the recently developed *B*-spline *R*-matrix code [11–14], where a *B*-spline basis is employed to represent the continuum functions. In the present work, particular emphasis was placed on the accuracy of the target description. The distinct feature of our approach is the use of *term-dependent nonorthogonal* orbitals in the description of the target states. This allows us to optimize the various atomic wave functions *individually*. Furthermore, since we do not impose orthogonality constraints between the continuum functions and the atomic orbitals, we avoid potential inconsistencies between the continuum and the bound parts of standard close-coupling expansions, even in the case of large configuration expansions and numerous correlated pseudo-orbitals.

II. COMPUTATIONAL DETAILS

The theory and a general description of the present technique for the case of photonic collisions were already given in detail in our previous calculation of photoionization of Li [12]. Hence we only summarize the scattering model and the approximations made specifically in the present work for low-energy photodetachment of negative atomic oxygen ions.

A. Target wave functions

The target states of neutral oxygen were generated with the *B*-spline box-based close-coupling method [15]. Specifically, the close-coupling expansion had the form

$$\Phi(2s^2 2p^3 nl;LS) = \mathcal{A} \sum_{i,L'S'} \{\varphi(2s^2 2p^3;L'S')P(n_i l_i)\}^{LS} + \sum_{n'l'} \chi(2s2p^4 n'l';LS) + \sum_{n'l',n''l''} \chi(2s^2 2p^3 n'l'n''l'';LS). \quad (1)$$

The first sum in this expansion represents the physical states, whereas the last two terms represent the core-valence correlation. The inner-core correlation was introduced by using a multiconfiguration Hartree-Fock (MCHF) expansion for the $\varphi(2s^2 2p^3)$ core states. The core-valence correlation is very important for an accurate representation of the valence orbitals, whereas the inner-core correlation was found to be important to accurately describe the $2s^2 2p^4$ and $2s2p^5$ states, as well as the Rydberg limits corresponding to $O^+(2s^2 2p^3)$.

We first generated the spectroscopic $1s$, $2s$, and $2p$ orbitals from term-averaged Hartree-Fock calculations for the $1s^2 2s^2 2p^3$ configuration. Then the $\varphi(2s^2 2p^3)$ core states were obtained in the MCHF approach [16] with a set of correlation functions $\bar{n}\ell\,(\ell=0-3)$, designed specifically to represent inner-core correlation. The CI expansions for each term contained the principal configuration $2s^2 2p^3$ along with all one-electron and two-electron excitations from the $2s$ and $2p$ subshells. The convergence of the multiconfiguration expansions for the $2s^2 2p^3$ core states was found to be very slow. Using extensive expansions for the core states, however, may lead to large final expansions (1) for the target wave functions, which may be difficult to handle in practice. We therefore explored different target models by limiting the CI expansions for the $2s^2 2p^3$ core states to those terms with coefficients of magnitude larger than some cutoff parameters indicated in Table I. In this approach, the target models differ mostly by the amount of inner-core correlation incorporated into the wave functions.

TABLE I. Parameters of the $2p^4\ ^3P$ ground state in different target models.

	Model 1	Model 2	Model 3
Energy (a.u.)	−74.94211	−74.95554	−74.97403
Cutoff parameter	0.05	0.025	0.01
Number of configurations	32	71	190

In the next step, we generated another independent set of correlation functions $\bar{n}\ell\,(\ell=0-3)$, this time designed to represent the core-valence correlation. This was done for each *LS* term separately by optimizing the lowest $2p^3 3s$, $2p^3 3p$, and $2p^3 3p$ states for a given term on the basis of the configurations indicated in the last two terms of expansion (1). In order to simplify the final target expansions, configurations with coefficients of magnitude less than 0.005 were ultimately dropped. Note that the correlation orbitals to represent the core-valence correlation are much more extended than those to account for inner-core correlation in the $2s^2 2p^3$ core states, and that the two sets are not orthogonal to each other. Such a procedure to represent various types of correlation effects with different nonorthogonal sets of correlation orbitals generally leads to more compact and, at the same time, to more accurate configuration expansions for the target states. As an example, the average number of configurations in the final target CI expansions is illustrated in Table I for the expansion of the ground-state wave function.

The unknown functions for the outer valence electron $P(n\ell)$ were then expanded in the *B*-spline basis and the corresponding equations were solved subject to the condition that the wave functions vanish at the *R*-matrix boundary. The details of this procedure are given in Ref. [15]. The radial functions $P(n\ell)$ were chosen orthogonal to the $2s$ and $2p$ spectroscopic orbitals but not to the correlation orbitals. In this case, the $2s$ and $2p$ orbitals were generated again for each term, allowing for complete term-dependent relaxation.

The above scheme yields nonorthogonal, term-dependent valence orbitals for each *LS* term, i.e., we directly include the term-dependent effects in our target wave functions. The number of physical states we can generate in this method depends upon the size of the *R*-matrix box. Choosing $a=45a_0$ (where a_0 is the Bohr radius) yields a good description for all low-lying states of atomic oxygen up to $n=5$. Table II compares our target excitation energies with the experimental values. The agreement is better than 90 meV for all states, and hence we believe that the target wave functions include the most important correlation corrections. Note that the excitation energies for all target models indi-

TABLE II. Comparison between the present *ab initio* and observed (NIST Atomic Spectra Database, http://physics.nist.gov) energies (in eV) of the physical oxygen states included in the close-coupling expansion.

State	Theory	Observed	Difference
$2s^22p^4\ ^3P$	0	0	0
$2s^22p^4\ ^1D$	1.950	1.957	−0.007
$2s^22p^4\ ^1S$	4.180	4.180	0.000
$2s^22p^3(^4S^o)3s^3S^o$	9.581	9.511	0.070
$2s^22p^3(^4S^o)3p^3P$	11.032	10.979	0.053
$2s^22p^3(^4S^o)4s^3S^o$	11.936	11.920	0.016
$2s^22p^3(^4S^o)3d^3D^o$	12.086	12.077	0.009
$2s^22p^3(^4S^o)4p^3P$	12.362	12.349	0.013
$2s^22p^3(^2D^o)3s^3D^o$	12.609	12.530	0.079
$2s^22p^3(^4S^o)5s^3S^o$	12.693	12.687	0.006
$2s^22p^3(^2D^o)3s^1D^o$	12.796	12.718	0.078
$2s^22p^3(^4S^o)4d^3D^o$	12.752	12.749	0.003
$2s^22p^3(^2P^o)3s^3P^o$	14.198	14.114	0.084
$2s^22p^3(^2P^o)3s^1P^o$	14.449	14.362	0.087
$2s^22p^3(^2D^o)4s^1D^o$	15.231	15.215	0.016
$2s^22p^3(^2D^o)3d^3P^o$	15.313	15.281	0.032
$2s^22p^3(^2D^o)3d^1F^o$	15.406	15.405	0.001
$2s^22p^3(^2D^o)3d^1D^o$	15.410	15.404	0.006
$2s2p^5\ ^3P^o$	15.701	15.650	0.051
$2s^22p^3(^2D^o)4d^1F^o$	16.075	16.075	0.000
$2s^22p^3(^2D^o)4d^3P^o$	16.111	16.105	0.006
$2s^22p^3(^2P^o)4s^3P^o$	16.864	16.800	0.064
$2s^22p^3(^2P^o)4s^1P^o$	16.928	16.896	0.032
$2s^22p^3(^2P^o)3d^1P^o$	17.106	17.098	0.008
$2s^22p^3(^2P^o)4d^1P^o$	17.772	17.767	0.005

cated in Table I are very similar; only the absolute energies are different.

Along with these physical states, the above scheme also provides a set of pseudostates. The lower-lying states represent coupling to the remaining bound states while the others represent coupling to the O^+ continuum. The number and density of pseudostates again depend upon the size of the *B*-spline basis. Although we could use small effective bases with an exponential grid of knots [15] in the bound-state calculations alone, we employ the same *B*-spline basis in the bound and the scattering calculations. In order to also provide a good description for all scattering orbitals up to 1 Ry of energy, we chose *B*-splines of order 8 on a semilogarithmic grid of knots with a maximum stepsize of $1a_0$. These conditions, together with the size of the *R*-matrix box, required 98 splines in the present calculations.

B. Scattering calculations

The photodetachment calculations were carried out using the new *R*-matrix code [11]. As mentioned above, nonorthogonal sets of orbitals are used to describe both the target states and the *R*-matrix continuum basis functions, and a *B*-spline basis is used to represent the continuum functions in the internal region. As in the standard *R*-matrix method [17], the wave function of the $(N+1)$-electron system in the internal region with $0<r<a$ is expanded in terms of energy-independent functions

$$\Psi_k = A\sum_{ij} a_{ijk}\bar{\Phi}_i u_j(r) + \sum_j b_{jk}\chi_j, \tag{2}$$

where the $\bar{\Phi}_i$ are channel functions formed from the *N*-electron target states Φ_i (physical and pseudo) included in the close-coupling expansion, and the u_j are radial basis functions describing the motion of the scattering (here the detached) electron. The χ_j are $(N+1)$-electron bound configurations. Some of these must be included for completeness of the expansion if orthogonality restrictions are imposed, but they can also represent short-range correlation effects. In our implementation of the *R*-matrix method, the radial functions u_j are expanded in the spline basis as

$$u_j(r) = \sum_i \bar{a}_{ij} B_i(r), \tag{3}$$

where the coefficients $\bar{a}_{ij}$ [which now replace the coefficients a_{ijk} and b_{jk} in Eq. (2)] are found by diagonalizing the $(N+1)$-electron Hamiltonian inside the *R*-matrix box of radius *a*. Using the *B*-spline basis leads to a generalized eigenvalue problem of the form

$$\boldsymbol{Hc} = E\boldsymbol{Sc}, \tag{4}$$

where $\boldsymbol{S}$ is the overlap matrix. If orthogonality conditions are imposed on the scattering orbitals, $\boldsymbol{S}$ reduces to a banded matrix consisting of overlaps between individual *B*-splines. In the more general case of nonorthogonal sets of orbitals, however, its structure is more complicated [12]. For an accurate determination of the electron flux through the boundary, we do not impose any boundary conditions on the u_j functions at the outer edge of the box. Consequently, the Bloch operator [17] is added to make the interaction matrix Hermitian in the internal region. The amplitudes of the scattering wave functions in the various channels at the boundary, which are needed for the construction of the *R*-matrix, are then given by the coefficient of the last spline, which is the only nonzero spline at the boundary. An important property of a *B*-spline basis is its *effective completeness* on the interval spanned by the knot sequence. Consequently, no Buttle correction [17] to the *R*-matrix elements is required in the present approach.

Since we only imposed limited orthogonality conditions on the scattering orbitals to the $1s$, $2s$, and $2p$ core orbitals (see the previous section), the introduction of $(N+1)$-electron terms to compensate for these orthogonality restrictions is avoided. The scattering parameters were then found by employing the ASYPCK program [18] to match the inner-region solutions at $r=a$ to the asymptotic solutions for $r>a$.

The initial $O^-(2p^5\ ^2P^o)$ state was calculated using the same close-coupling expansion (2) as in the scattering calculations, this time imposing a boundary condition of zero at $r=a$. In this case the expansion (2) also contained the set of

TABLE III. *B*-spline *R*-matrix (BSR) scattering models used in the present work. The number of coupled states is indicated after the dash.

	BSR-3	BSR-17	BSR-60	BSR-108	Expt.
Number of target states	3	17	60	108	
Electron affinity (eV)	1.451	1.455	1.478	1.491	1.461[a]
$\alpha(2p^4\ ^3P)$ $[a_0^3]$	0.0	1.49	2.24	4.07	5.2±0.4[b]
$\alpha(2p^4\ ^1D)$ $[a_0^3]$	0.0	0.90	2.78	2.78	5.19[c]
$\alpha(2p^4\ ^1S)$ $[a_0^3]$	0.0	0.96	3.40	3.40	5.66[c]

[a]Neumark *et al.* [20].
[b]Alpher and White [19].
[c]Calculated with the full *B*-spline pseudospectrum.

$(N+1)$-electron bound configurations obtained from the direct MCHF calculations of the $2p^5\ ^2P^o$ state. Such a scheme allows us to include accurately both short-range and long-range correlations in the initial state. Generally, the effect of core relaxation is very large in open-shell anions, and the outer p orbital is much more diffuse in the anions than in the corresponding neutral atoms. Direct MCHF calculations predominantly optimize the wave function at small radii, whereas the close-coupling terms in the expansion (2) are intended for a more accurate description of the $2p^5\ ^2P^o$ state at large distances. The $2p^5\ ^2P^o$ electron affinities obtained in different scattering models are listed in Table III. We notice good agreement with the experimental data, although inclusion of additional scattering channels leads to a slight overestimate of this value compared to experiment [19]. In all photodetachment calculations, we used the experimental value for the electron affinity. The dipole matrix elements between the initial state and the final continuum functions were calculated on the basis of nonorthogonal orbitals with full inclusion of relaxation effects.

In order to explore the dependence of the predicted photodetachment cross sections on the number of scattering channels and the polarization of the target, we used the four scattering models listed in Table III. The simplest BSR-3 model only includes the three $2p^4$ states and hence does not account for any target polarization by the scattering electron. The BSR-17 scattering model includes 14 triplet and singlet states of O up to the $2s^22p^3(^4S^o)4d^3D^o$ state, plus five states $[2s^22p^3(^2P^o)3s^{1,3}P^o$, $2s2p^5\ ^3P^o$, and two $^3D^o$ pseudostates]. These additional states provide considerable individual contributions to the polarizability of the $2p^4$ states. We also note that the present box-based *B*-spline calculations with a large number of splines provide an adequate representation of the bound and continuum spectrum for the oxygen atom. For example, if we calculate the polarizability of the ground state including all pseudostates generated in the present scheme, we obtain $5.18a_0^3$, which is very close to the experimental value [20]. The contribution of the individual physical and pseudostates, however, is relatively small, usually less than $0.1a_0^3$. This reflects the broad distribution of the generalized oscillator strengths over a wide energy range found in the photoionization measurements of oxygen atoms [3]. On the other hand, it prevents the effective use of these pseudostates in scattering calculations, because their full account would lead to very large close-coupling expansions. In our more extensive BSR-60 and BSR-108 model, we therefore select only states that give substantial contributions to the polarization of the target. The BSR-60 model contains all physical states indicated in Table II plus the pseudostates whose individual contribution to the polarizability of the $2p^4$ states is greater than $0.05a_0^3$. The BSR-108 model additionally contains the pseudostates whose individual contribution to the polarizability of the $2p^4\ ^3P$ ground state is greater than $0.025a_0^3$.

III. RESULTS

In the nonrelativistic *LS* approximation used in the present work, the $2p$ photodetachment of $O^-(2p^5\ ^2P^o)$ occurs in three partial waves, ^2S, ^2P, and ^2D. The principal scattering channels are $2p^4(^3P;\ ^1D;\ ^1S)ks$ and kd.

Figure 1 compares the total cross sections obtained with different target models. Note that short-range correlation effects are extremely important in the present case. The low-correlated target states in "model 1" lead to spurious structures near the $2p^4$ thresholds. In this case, the

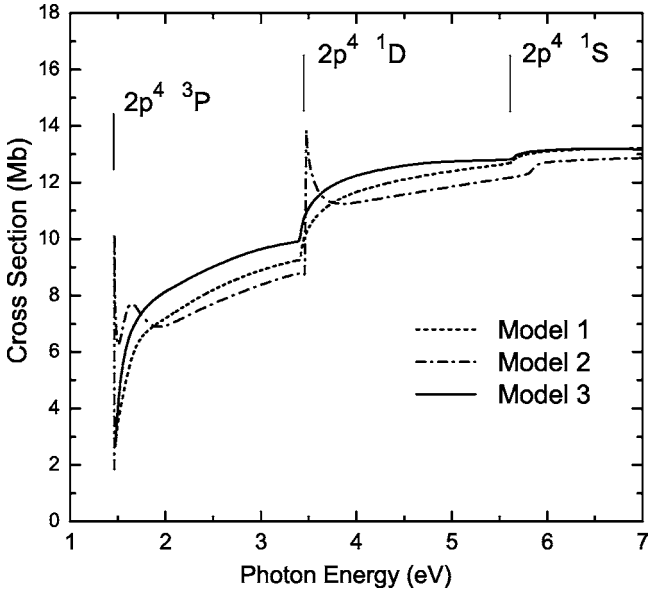

FIG. 1. Photodetachment cross section for different target models (see Table II) as a function of the photon energy. The target thresholds are indicated by the vertical lines.

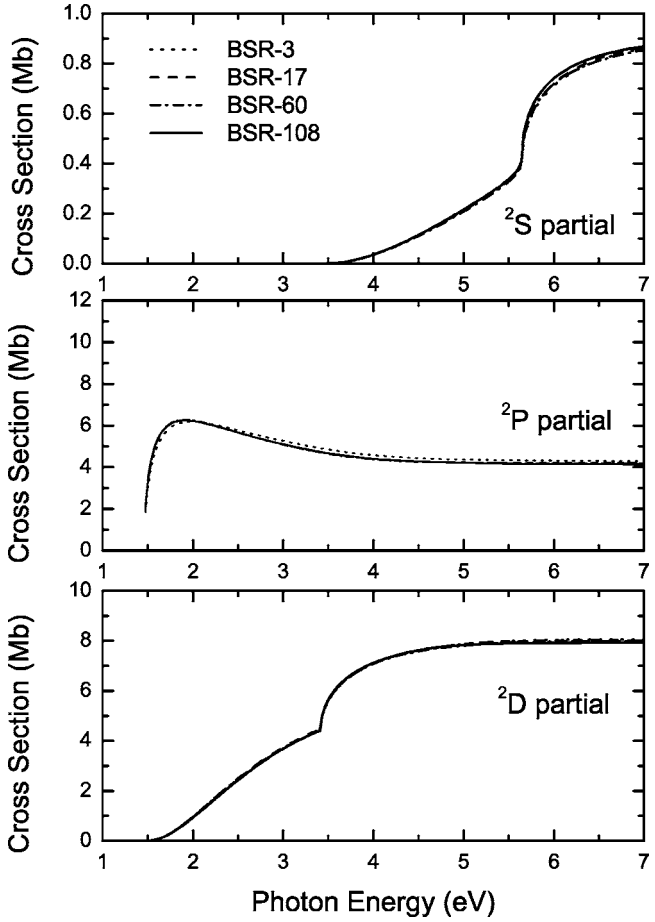

FIG. 2. Partial-wave contributions to the photodetachment cross section for different collision models (see Table III) and target model 3.

$(N+1)$-electron system becomes overcorrelated relative to the target description when the number of scattering channels is increased. The very same effect is responsible for a spurious threshold spike in the calculated elastic cross section for the e-O collision problem [13], where the target wave functions correspond to model 1 in the present calculations. A balanced description of the correlation in the N-electron target and the $(N+1)$-electron scattering function is a common problem for close-coupling calculations in the near-threshold regime. For example, correlation effects in the ground state strongly affect the position and height of the $(3s^2np\ ^2P)$ shape resonance in e-Mg collisions [14]. Note that this balance only concerns the *physics of correlation* included in the target and the collision problems. Sometimes close-coupling expansions with orthogonal target (pseudo) and continuum orbitals may also suffer from *numerical* inconsistencies due to the use of approximate target wave functions. If necessary, these can be eliminated using the method described by Gorczyka *et al.* [22], but they are not a problem in our approach.

In contrast to common perception, we do not find a significant dependence of the calculated photodetachment cross section on the degree to which the polarization of the target state was accounted for. This is illustrated in Fig. 2, where the partial cross sections obtained in different scattering models are compared for the most correlated target model 3.

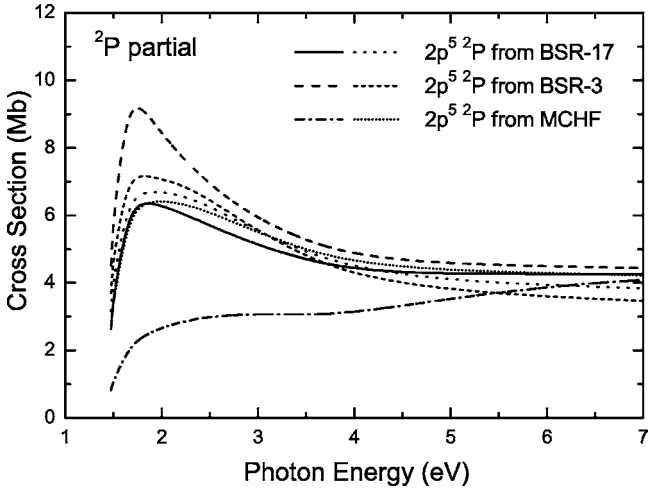

FIG. 3. Contribution from the ^2P partial wave to the photodetachment cross section for different models of the initial $O^-(2p^5\ ^2P^o)$ state, as obtained in the BSR-17 collision model and target model 2. The two lines for each initial-state model represent the length and velocity results, respectively.

Each scattering model differs by the number of scattering channels and, consequently, by the polarization of the ground state accounted for. However, we found a much stronger dependence of the photodetachment cross section on the scattering model when the less correlated target descriptions of model 1 and model 2 were used. This dependence is actually related to the problem of a balanced description of correlation in the N-electron target and the $(N+1)$-electron scattering functions discussed above, rather than to the polarization of the target states.

We also found a strong dependence of the photodetachment cross sections on the description of the initial $O^-(2p^5\ ^2P^o)$ state. This is illustrated in Fig. 3, where results obtained with different wave functions for the initial state are compared. The latter differ mainly by the description of the initial state at large radii. Whereas the velocity-form results are fairly close to each other, the length-form results differ considerably at low energies. This can be explained by the fact that the outer p orbital in the negative O^- ion is very diffuse. For such a case, the close-coupling expansion (2) provides a more accurate description of the $O^-(2p^5\ ^2P^o)$ wave function at large distances than direct MCHF calculations that minimize the energy. As we see from Fig. 3, the most consistent results are obtained when the initial state is calculated within the same close-coupling expansion as the scattering model.

Figure 4 compares our cross sections for $2p$ photodetachment to the available experimental and theoretical data. Our final results were obtained in the BSR-108 collision model with target model 3. We note good agreement with the experimental data regarding the energy dependence of the cross section. Two step structures in the curves are due to the opening of new thresholds. Close agreement is also seen between the length and velocity forms of our predictions. However, our absolute numbers for the photodetachment cross sections exceed the experimental values [1,2] by about 40%. Although the measurements [1] were carried out 45 years

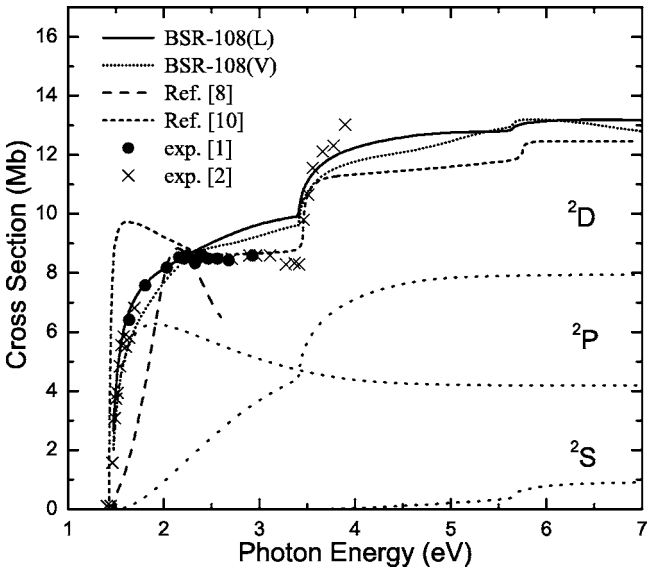

FIG. 4. Length-form (L) and velocity-form (V) photodetachment cross sections from the present work compared to the experimental data of Refs. [1,2]. The published experimental data were multiplied by 1.4. Also shown are the length-form results from the *R*-matrix calculations of Refs. [8,10], as well as the contributions from individual partial waves to the present length-form results.

ago, it is worth noting that these data are still being used today to normalize relative data from photodetachment experiments. Our previous calculations of B^- and C^- photodetachment [21] also showed excellent agreement with the experimental data regarding the energy dependence, but the absolute theoretical values exceeded the experimental cross sections by about 35%. Interestingly, both the B^- and C^- measurements for the photodetachment cross sections were normalized to the O^- data of Ref. [1]. The very similar differences obtained in three independent calculations with absolute experimental values based upon a *single* cross-normalization suggests a possible systematic error of about 35% in Refs. [1,2].

We also see from Fig. 4 that our cross sections agree well with the *R*-matrix results of Wu *et al.* [10] in respect to the absolute values. However, the latter results exhibit a different threshold behavior. The energy of the ground state in Ref. [10] was −74.9540 Hartree, i.e., close to that of our target model 2. Nevertheless, the near-threshold energy dependence of the photodetachment cross sections obtained in Ref. [10] is closer to our cross sections obtained with an even simpler description of the target, notable the BSR-3 model in Fig. 3. In their description of the target, Wu *et al.* used only correlated orbitals, which were optimized on the lowest $2p^4$ state. This may provide a good description of short-range correlations, but it is likely not sufficient to ensure an accurate description of the initial $2p^5\ ^2P$ state at large distances, even though they used a large *R*-matrix box of $80a_0$. As discussed above, the accurate description of the initial state at large distances is very important for the present case and may strongly influence the near-threshold results for the photodetachment cross sections (see Fig. 3).

The cross section obtained in the eigenvalue *R*-matrix calculation by Miecznik and Greene [8] exhibits a very different energy behavior than both experiment and the other theoretical results. Note, however, that Miecznik and Greene only considered the $2p^4(^3P)\varepsilon s$ detachment channel, since the partial cross sections associated with *d* waves were suspected to be strongly suppressed at small energies by a centrifugal barrier. Hence their results should only be compared with the ^2P partial data presented in Fig. 4. Nevertheless, we note large discrepancies, especially concerning the slope in the near-threshold energy dependence of the cross section. This may be related to the small *R*-matrix radius of $12a_0$ chosen by Miecznik and Greene, which prevents an accurate representation of the initial state at large distances. Furthermore, as seen from Fig. 4, the $2p^4(^3P)\varepsilon d\,^2D$ detachment channel quickly gains intensity with increasing photon energy and becomes comparable to the $2p^4(^3P)\varepsilon s$ channel at the $2p^4(^1D)$ threshold. At even larger energies a significant contribution also comes from the $2p^4(^1D)\varepsilon s$ photodetachment channel. Miecznik and Greene concluded that the calculated cross section depends significantly on the target polarization effects accounted for, because the largest effect comes from the $2s \rightarrow np$, $2p \rightarrow ns$, and $2p \rightarrow nd$ terms in their multiconfiguration target wave functions. The target polarization in their formulation, however, was essentially a *short-range* effect. All electron-electron and electron-nuclear interactions were only evaluated inside the reaction zone, whereas the potential was purely centrifugal beyond $a=12a_0$. We therefore believe that this approach does not allow to draw an unambiguous conclusion about the importance of the target polarization, unless one (re)defines polarization effects as any dipole interaction between the projectile and the target.

IV. SUMMARY

We have presented a detailed investigation of the O^- photodetachment problem, with particular emphasis on the dependence of the predicted partial and total cross sections on the scattering model and the accuracy of the target description. The calculations were performed with a new extended version of the *R*-matrix method, where nonorthogonal sets of orbitals are extensively used in both the target description and the representation of the scattering functions. This technique allows for term-dependent optimization of the bound orbitals, generally leading to more accurate target descriptions than those used in previous calculations. It also provides a systematic way to account for inner-core and core-valence correlation. Abolishing the orthogonality constraints imposed on the scattering orbitals guarantees a numerically consistent treatment of the *N*-electron target and the $(N+1)$-electron collision problems, even when numerous pseudo-orbitals and large configuration expansions are employed.

We found that the theoretical O^- photodetachment cross sections in the near-threshold regions strongly depend on the inner-core correlation incorporated into the target wave functions. This is particularly important when studying the convergence of the close-coupling expansion. When the number of scattering channels is increased more and more, the $(N+1)$-electron system ultimately becomes overcorrelated relative to the target description. This overcorrelation may

lead to the appearance of pseudoresonances in the threshold regime.

We only found a small dependence of the calculated photodetachment cross section on the degree to which the polarization of the target states was accounted for. We therefore suggest that the influence of polarization in the $h\nu+O^-$ process is small compared to the strong short-range interaction of the scattering (detached) electron with the $2p^4$ open shell. This assessment contradicts previous conclusions [4–6] that the target polarization is very important in the treatment of O^- photodetachment. Note, however, that the model polarization potentials in the latter works were used to simulate *all* correlation corrections, not just those due to the target polarization. The use of accurate target wave functions in the present *ab initio* calculations, on the other hand, allowed us to clearly distinguish between the influence of short-range and long-range correlations. We also emphasize that the *B*-spline box-based close-coupling method provides a pseudostate spectrum, which reproduces the distribution of the generalized oscillator strength over the discrete states and the continuum more accurately than previous methods.

In summary, the present *B*-spline *R*-matrix calculations, together with the recent independent work by Wu *et al.* [10], suggest a possible systematic error of about 35% in the *only absolute measurement* by Smith [1] performed many years ago. This is an important issue because the latter experimental data are still being used today to normalize relative data from current photodetachment experiments. New absolute measurements of the O^- photodetachment cross sections seem highly desirable to either resolve or confirm the current disagreement between experiment and theory.

ACKNOWLEDGMENTS

This work was supported by the United States National Science Foundation under Grant Nos. PHY-0311161 and PHY-0244470.

[1] S. J. Smith, *Proceedings of the ICPIG*, 4th Uppsala, IC219 (1959).
[2] L. M. Branscomb, S. J. Smith, and G. Tisone, J. Chem. Phys. **43**, 2906 (1965).
[3] J. Berkowitz, J. Phys. B **32**, 583 (1997).
[4] W. R. Garrett and H. T. Jackson, Phys. Rev. **153**, 28 (1967).
[5] R. J. W. Henry, Phys. Rev. **162**, 56 (1967).
[6] K. L. Vo, N. Feautrier, M. Le Dourneuf, and H. Van Regemorter, J. Phys. B **5**, 1506 (1972).
[7] R. L. Chase and H. P. Kelly, Phys. Rev. A **6**, 2150 (1972).
[8] G. Miecznik and C. H. Greene, Phys. Rev. A **53**, 3247 (1996).
[9] T. Suzuki and T. Kasuya, Phys. Rev. A **36**, 2129 (1987).
[10] J.-H. Wu, J.-M. Yuan, and K. L. Vo, Chin. Phys. **12**, 1391 (2003).
[11] O. Zatsarinny, Comput. Phys. Commun. **174**, 273 (2006).
[12] O. Zatsarinny and C. Froese Fischer, J. Phys. B **33**, 313 (2000).
[13] O. Zatsarinny and S. S. Tayal, J. Phys. B **34**, 1299 (2001).
[14] K. Bartschat, O. Zatsarinny, I. Bray, D. V. Fursa, and A. T. Stelbovics, J. Phys. B **37**, 2617 (2004).
[15] O. Zatsarinny and C. Froese Fischer, J. Phys. B **35**, 4669 (2002).
[16] C. Froese Fischer, T. Brage, and P. Jönsson, *Computational Atomic Structure: An MCHF Approach* (Institute of Physics Publishing, Bristol and Philadelphia, 1997).
[17] P. G. Burke and K. A. Berrington, *Atomic and Molecular Processes: An R-Matrix Approach* (Institute of Physics Publishing, Bristol, 1993).
[18] M. A. Crees, Comput. Phys. Commun. **19**, 103 (1980).
[19] R. A. Alpher and D. R. White, Phys. Fluids **2**, 153 (1959).
[20] D. M. Neumark, K. R. Lykke, T. Andersen, and W. C. Lineberger, Phys. Rev. A **32**, 1890 (1985).
[21] O. Zatsarinny and T. W. Gorczyca, *Abstracts of XXIII ICPEAC*, Stockholm (2003), We026, Th006.
[22] T. W. Gorczyca, F. Robicheaux, M. S. Pindzola, D. C. Griffin, and N. R. Badnell, Phys. Rev. A **52**, 3877 (1995).